

Annealing mechanisms of intrinsic defects in 3C-SiC: a theoretical study

Michel Bockstedte, Alexander Mattausch, and Oleg Pankratov

Lehrstuhl f. Theoretische Festkörperphysik, Universität Erlangen-Nürnberg, Staudtstr. 7B2, D-91058 Erlangen, Germany

(Dated: October 31, 2018)

The annealing kinetics of mobile intrinsic defects is investigated by an *ab initio* method based on density functional theory. The interstitial-vacancy recombination, the diffusion of vacancies and interstitials to defect sinks (e.g. surfaces or dislocations) as well as the formation of interstitial-clusters are considered. The calculated migration and reaction barriers suggest a hierarchical ordering of competing annealing mechanisms. The higher mobility of carbon and silicon interstitials as compared to the vacancies drives the annealing mechanisms at lower temperatures including the vacancy-interstitial recombination and the formation of interstitial carbon clusters. These clusters act as a source for carbon interstitials at elevated temperatures. In p-type material we discuss the transformation of the silicon vacancy into the more stable vacancy-antisite complex as an annealing mechanism, which is activated before the vacancy migration. Recent annealing studies of vacancy-related centers in irradiated 3C- and 4H-SiC and semi-insulating 4H-SiC are interpreted in terms of the proposed hierarchy of annealing mechanisms.

PACS numbers: 61.72.Ji, 61.72.Cc, 66.30.-h

I. INTRODUCTION

The unique features of silicon carbide, such as the wide band gap and the electrical and thermal stability, recommend this semiconductor for high power, high frequency and high temperature applications. As for any semiconductor, unwanted defects are introduced into this material by growth processes and ion-implantation of dopants. Besides the primary defects – interstitials and vacancies – secondary defects such as antisites and defect clusters are created. Thermal annealing is applied to reduce these defects to an inevitable abundance. Thereby the high electron mobility is restored and the electrical activation of dopants is achieved.

The annealing properties of intrinsic and impurity-related defect centers were studied in irradiated SiC by various experimental techniques, for instance electron spin resonance techniques (EPR), deep level transient spectroscopy (DLTS), photoluminescence spectroscopy (PL) and positron annihilation spectroscopy (PAS). Some of the reported centers persist up to a temperature range of 1300°C-1700°C. Examples for such defects are the PL-centers D_I (Refs. 1,2,3) and D_{II} (Refs. 4,5) as well as the DLTS-center Z_1/Z_2 and E_1/E_2 in 4H- and 6H-SiC (Ref. 6) respectively. The microscopic origin of most of the centers is still investigated. The PL-centers P-U (Ref. 7) and D_{II} have been interpreted as carbon interstitials⁷ or interstitial clusters,⁴ due to their carbon-related localized vibrational modes (LVMS) with frequencies above the SiC bulk-spectrum. Depending on the experimental conditions some of these centers even grow in intensity during the heat treatment in a temperature range between 500°C and 1200°C, when others (e.g. vacancy-related centers) gradually vanish.^{6,8,9}

Vacancies and interstitials act as vehicles for otherwise immobile point defects. Defect clusters may only be diminished by reacting with or separating into these mobile entities. Vacancy related defects have been stud-

ied by PAS^{6,10,11,12,13} and EPR^{14,15,16,17} in irradiated material. In PAS,¹⁰ defects related to silicon and carbon vacancies can be distinguished thanks to a considerable difference of the positron lifetimes, as predicted by theory.^{18,19} EPR-centers have also been identified as isolated silicon^{14,15,17} and carbon^{16,20,21} vacancies and the assignment has been verified theoretically.^{14,22,23,24} Characteristic differences were observed for the annealing behavior of carbon and silicon vacancies in irradiated SiC. A lower annealing temperature ($\sim 500^\circ\text{C}$) was deduced for the carbon vacancy by PAS¹⁰ and EPR.¹⁶ The annealing of the silicon vacancy occurs in several stages, at 150°C, 350°C and 750°C (the final annealing stage) as observed by EPR¹⁷ in 3C-SiC in agreement with PAS¹² data. In irradiated n-type 4H- and 6H-SiC, however, additional annealing stages of centers related to a silicon vacancy were observed by PAS^{6,25} at temperatures up to 1450°C. This finding was explained by the formation of stable nitrogen-vacancy complexes. On the other hand, a vacancy-antisite complex was identified by EPR experiments²⁶ in irradiated n-type 6H-SiC annealed above 750°C. An EPR-center with similar properties was also identified in 3C-SiC.²⁷ The center evolves from the silicon vacancy as a consequence of the vacancy's metastability in p-type and intrinsic material predicted previously by theory.^{28,29} In both experiments the signature of the silicon vacancy was absent. Other experiments^{20,30} indicate that the carbon and silicon vacancies possess a higher thermal stability in semi-insulating than in irradiated SiC. A comprehensive interpretation of the annealing experiments in terms of simple mechanisms is lacking so far. In particular, the role that interstitials and vacancies play in the reported annealing stages is not known. Furthermore, the Fermi-level effect on the annealing behavior of the charged defects has not been clarified.

In the present paper we analyze the annealing of vacancies and interstitials in 3C-SiC at a microscopic level.

We study the effect of clustering on the defect kinetics in case of carbon interstitials. An *ab initio* method within the framework of density functional theory (DFT) is employed to calculate the migration barriers and recombination paths. The aggregation of carbon interstitials is analysed and the dissociation energy needed to re-emit a single carbon interstitial is calculated. A hierarchy of annealing mechanisms (cf. Fig. 1) is proposed on the basis of the calculated barriers and dissociation energies at different doping conditions. For the carbon-related defects we show that the vacancy-interstitial recombination and the diffusion-limited annealing of carbon interstitials are the first two annealing stages in this hierarchy followed by the diffusion-based annealing of carbon vacancies. Besides the diffusion-limited vacancy-interstitial recombination the clustering of carbon interstitials may facilitate their annealing. Thermally stable carbon clusters re-emit carbon interstitials at high temperatures thereby contributing to the kinetics of other thermally stable defects.

While the Fermi-level effect is not pronounced in the case of carbon vacancies and interstitials, it substantially affects the annealing of silicon vacancies and interstitials. This is related to the metastability of the silicon vacancy in p-type and intrinsic material and the existence of two different interstitial configurations in p-type and intrinsic or n-type SiC. For intrinsic (compensated) SiC, the vacancy-interstitial recombination precedes the metastability-related transformation of the vacancy into the carbon vacancy-antisite complex, which in a next stage either dissociates or anneals via a diffusion-limited mechanism. For p-type conditions the transformation-induced annealing dominates over the diffusion-limited vacancy-interstitial recombination. In n-type material a diffusion-limited annealing of the silicon vacancy should follow the vacancy-interstitial recombination in the hierarchy of annealing mechanisms.

The outline of the paper is as follows. Preceded by a description of the method in Section II, we summarize the migration mechanisms of interstitials and vacancies in Section III. We also review the metastability of the silicon vacancy there and analyze the kinetic aspects of this metastability with emphasis on Fermi-level effects. Section IV treats the stable Frenkel pairs and the recombination paths of vacancies and interstitials. In Section V the properties of carbon interstitial clusters and their dissociation energies are described. The hierarchy of annealing mechanisms is outlined and discussed in the light of recent experiments in Section VI.

II. METHOD

We employ the plane wave pseudopotential program package FHI96MD³¹ based on density functional theory^{32,33} and the local density approximation^{34,35} (LDA) for the exchange-correlation functional. Spin effects are included within the LSDA where noted. Defects and

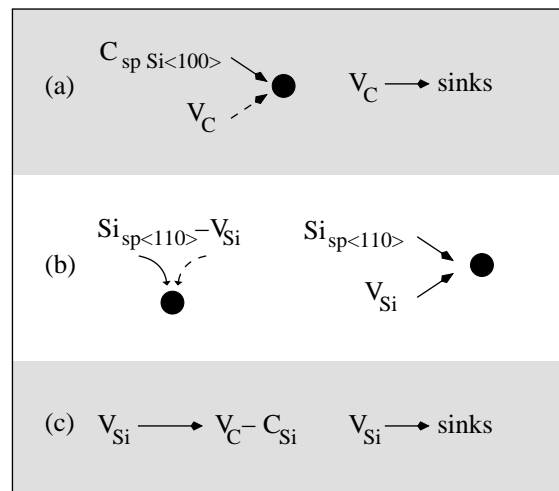


FIG. 1: Possible annealing paths of vacancies: (a) carbon vacancy: recombination of a carbon split-interstitial ($C_{sp\langle 100 \rangle}$) with a carbon vacancy (V_C) and the migration of carbon vacancies to sinks, (b) silicon vacancy: Frenkel pair recombination (compensated and n-type material) and diffusion limited recombination with split interstitial ($Si_{sp\langle 110 \rangle}$), and (c) annealing by the metastability induced transformation into a carbon vacancy-antisite complex (p-type and compensated material) and the migration of silicon vacancies to sinks (n-type).

their environment are described using large supercells, equivalent to 64 and 216 crystal lattice sites. A special k-point mesh³⁶ with 8 k-points in the Brillouin zone ($2 \times 2 \times 2$ -mesh) is used. For the description of Jahn-Teller distortions we performed the calculations in 216 atoms cell at the Γ -point in order to maintain the degeneracy of the defect levels. The ionization levels of charged defects were calculated following the approximate procedure proposed by Makov and Payne³⁷ to account for the error introduced by the compensating background. Especially for the highly charged interstitial defects this procedure leads to more consistent results.^{38,39} Norm-conserving carbon and silicon pseudopotentials of the Troullier-Martins type^{40,41} are employed. The carbon pseudopotential has been optimized⁴² for calculations with a small basis set. Extensive tests showed that a basis set of plane-waves with a kinetic energy up to 30 Ry yielded practically converged total energy differences. The coordinates of all atoms in the simulation cell have been relaxed. Tests have shown that all relevant relaxations are well contained within the simulation cells.

A. Formation energies

The abundance of defects is determined by their effective formation energy E_f . For charged defects, the latter depends on the doping conditions via the Fermi level μ_F and on the stoichiometry of the material via the carbon and silicon chemical potentials μ_C and μ_{Si} .

In equilibrium μ_C and μ_{Si} are not independent but related to the chemical potential of SiC μ_{SiC} through $\mu_{\text{SiC}} = \mu_C + \mu_{\text{Si}}$. Choosing μ_{Si} as a free parameter, we express it as $\mu_{\text{Si}} = \mu_{\text{Si}}^0 + \Delta\mu$ in terms of the chemical potential of crystalline Si and the difference $\Delta\mu$ to this value. The formation energy is given by

$$E_f = E_{\text{D, cell}} - n_{\text{Si}} \mu_{\text{Si}} - n_{\text{C}} \mu_{\text{C}} - n_e (E_{\text{V}} + \mu_{\text{F}}) \quad , \quad (1)$$

where $E_{\text{D, cell}}$ is the total energy of a super cell containing the defect and μ_{F} is defined relative to the valence band edge E_{V} . As outlined in Ref. 39 E_f may be conveniently written as

$$E_f = E_{\text{D}}^{n_e} - (n_{\text{Si}} - n_{\text{C}}) \Delta\mu - n_e \mu_{\text{F}} \quad . \quad (2)$$

In the above equations n_e is the number of excess electrons at the defect, n_{Si} and n_{C} are the numbers of silicon and carbon atoms in the supercell. The quantity $E_{\text{D}}^{n_e}$ is determined by $E_{\text{D}}^{n_e} = E_{\text{D, cell}}^{n_e} - n_{\text{C}} \mu_{\text{SiC}} - (n_{\text{Si}} - n_{\text{C}}) \mu_{\text{Si}}^0 - n_e E_{\text{V}}$ where the chemical potentials μ_{SiC} and μ_{Si}^0 are to a good approximation given by total energies of the perfect crystals. For E_{V} we take the value from a defect-free cell including a correction for the difference of the average potential in the defect and defect-free cell (c.f. Ref. 39). To ensure the stability of SiC, $\Delta\mu$ may only vary between the heat of formation of the corresponding polytype $H_{f, \text{SiC}}$ and 0, reflecting C-rich and Si-rich conditions respectively. $H_{f, \text{SiC}}$ only slightly depends on the polytype and amounts to 0.61 eV according to our findings choosing diamond as a reference for μ_{C} . This is slightly lower than the experimental value of 0.72 eV.

The ionization level of charged defects corresponds to the value of μ_{F} at which the defect alters its charge state. Thus it determines the defect charge state for given doping conditions. The ionization level is obtained from the formation energy by

$$\varepsilon(q_2|q_1) = E_{\text{D}}^{q_1} - E_{\text{D}}^{q_2} \quad . \quad (3)$$

Here q_1 and q_2 indicate the different charge states of the defect. Usually the charge state changes by one electron. However, in some cases⁴³ it may change by two when the additional electron-electron repulsion can be compensated by a lattice relaxation. This effect, known as the negative-U effect, leads to an attractive effective electron-electron interaction so that the ionization level $\varepsilon(q+1|q)$ appears below $\varepsilon(q|q-1)$. The realization of a charge state as a ground state for implies that the corresponding ionization levels and the occupied single particle levels are located below the conduction band edge. Even though a physical relevance of the Kohn-Sham levels is not rigorously founded by DFT, they reproduce the experimental quasi-particle band structure quite well. Yet, the calculated Kohn-Sham band gaps (1.2 eV and 2.2 eV in 3C- and 4H-SiC) are typically smaller than the experimental values (2.39 eV and 3.27 eV). In order to assess the defect charge states we follow a common practice and use the experimental value for the conduction band edge. However this procedure cannot unambiguously describe the

charge states that are stable only in the vicinity of the conduction band edge.

B. Defect migration

The analysis of migration and recombination paths starts with establishing the stable initial and final configuration. Then standard search methods are used to find the path between these configurations and to determine the saddle point. For the interstitial migration and the Frenkel-pair recombination we employ an implementation⁴⁴ of the ridge method of Ionova and Carter.⁴⁵ The ridge method performs an automatic search for the saddle point starting from the initial and final configuration. We repeat the search for all relevant charge states and analyze the obtained saddle points with respect to the geometry and the electronic structure. When the migration path depends on the occupation of defect states (near degeneracies, Jahn-Teller distorted ground states) this automatic search fails. This is relevant for the vacancy migration and the metastability-induced transformation of the silicon vacancy into a vacancy-antisite complex as discussed in Ref. 39. In these cases, we analyze the potential energy surfaces using the drag method. The procedure is outlined in Ref. 39, where we discuss the migration of the vacancies and their transition states in detail.

III. MIGRATION OF INTERSTITIALS AND VACANCIES

A. interstitials

In 3C-SiC a large number of interstitial configurations exists. Besides the tetrahedral and hexagonal interstitials also split-interstitials are relevant. In the latter the interstitial atom and the lattice atom share a lattice site in a dumbbell-like configuration, which is preferentially oriented along the $\langle 100 \rangle$ - or $\langle 110 \rangle$ -direction. Recently, we have analyzed these configurations for silicon and carbon interstitials.^{39,46} In particular, we have discerned the energetically most favorable sites. At these sites the interstitial migration starts and ends. Other interstitial configurations act as intermediate states along the migration path. The migration path and the energy barriers were investigated using a 64-atom cell and special k-points ($2 \times 2 \times 2$ Monkhorst-Pack mesh).

Among the carbon interstitials the two split-interstitials $\text{C}_{\text{sp}\langle 100 \rangle}$ and $\text{C}_{\text{spSi}\langle 100 \rangle}$ are the most favorable configurations. The split-interstitial $\text{C}_{\text{sp}\langle 100 \rangle}$ is centered at a carbon site and oriented in the $\langle 100 \rangle$ -direction as displayed in Fig. 2a. It is more favorable than the $\text{C}_{\text{spSi}\langle 100 \rangle}$ -interstitial which is a $\langle 100 \rangle$ -oriented silicon-carbon dumbbell at a silicon site. The electronic structure of the interstitials is discussed in detail in Ref. 39. The two interstitials are stable in positive and negative charge states.

TABLE I: Ionization levels of the mobile defects in 3C-SiC given relative to the valence band edge .

	$\varepsilon(1^+ 2^+)$	$\varepsilon(0 1^+)$	$\varepsilon(1^- 0)$	$\varepsilon(2^- 1^-)$
V_C	1.29	1.14	2.69	2.04
V_{Si}	–	0.18	0.61	1.76
V_C-C_{Si}	1.24	1.79	2.19	–
$Si_{sp\langle 110 \rangle}$	0.4	1.1	–	–
$C_{sp\langle 100 \rangle}$	0.6	0.8	1.8	–
$C_{spSi\langle 100 \rangle}$	0.4	0.7	1.9	2.3

TABLE II: Migration of carbon interstitials: energy barriers of nearest neighbor hops and second neighbor hops for the relevant charge states. The migration of $C_{sp\langle 100 \rangle}^0$ starts from the tilted configuration.

path	energy barrier [eV]			
	2^+	1^+	0	1^-
$C_{sp\langle 100 \rangle} \rightarrow C_{spSi\langle 100 \rangle}$	1.7	0.9	0.5	0.7
$C_{spSi\langle 100 \rangle} \rightarrow C_{sp\langle 100 \rangle}$	0.9	0.2	0.2	0.1
$C_{sp\langle 100 \rangle} \leftrightarrow C_{sp\langle 100 \rangle}$	1.4	0.9	0.5	0.6

The ionization levels of $C_{sp\langle 100 \rangle}$ and $C_{spSi\langle 100 \rangle}$ are given in Tab. I. Other interstitial sites, such as the hexagonal site and the tetrahedral sites, are higher in energy.

Two alternative migration paths have been found for the migration of carbon interstitials: a migration by second neighbor hops of $C_{sp\langle 100 \rangle}$ between adjacent carbon-sites and a migration by nearest neighbor hops between adjacent carbon and silicon lattice sites, going through the sequence $C_{sp\langle 100 \rangle} \rightarrow C_{spSi\langle 100 \rangle} \rightarrow C_{sp\langle 100 \rangle}$. The migration by second neighbor hops is indicated in Fig. 2.

The migration barriers for the two mechanisms are given in Tab. II. The nearest neighbor hop $C_{sp\langle 100 \rangle} \rightarrow C_{spSi\langle 100 \rangle}$ and the second neighbor hop $C_{sp\langle 100 \rangle} \rightarrow C_{sp\langle 100 \rangle}$ have similar migration barriers, except for the $C_{sp\langle 100 \rangle}^{2+}$. Small barriers are found for the migration of the positive, neutral and negative interstitials. The analysis of migration paths via other intermediate interstitial sites indicates that such paths are unlikely: the energy differences between $C_{sp\langle 100 \rangle}$ and these sites typically exceed the small migration barriers found for the above mechanisms.

Among the silicon interstitials the important sites are the tetrahedrally carbon coordinated site (Si_{TC}) and the (110)-oriented split-interstitial ($Si_{sp\langle 110 \rangle}$). The tetrahedral interstitial dominates in p-type material. Our analysis of the electronic structure shows³⁹ that it has no deep defect states within the band gap and therefore has a charge state of 4^+ . The bare silicon ion is efficiently screened by a crystal polarization. Considering the possible occupation of a defect state located slightly above the experimental conduction band edge we concluded in Ref 39 that the charge state 4^+ prevails for

TABLE III: Migration of silicon interstitials: energy barriers E_m in eV for different migration paths. The dominant migration paths are shown in Fig. 2. The charge state is indicated. See text for details.

	$Si_{TC}^{4+} \leftrightarrow Si_{sp\langle 100 \rangle}^{4+}$	$Si_{TC}^{4+} \leftrightarrow Si_{sp\langle 110 \rangle}^{4+}$	$Si_{TC}^{4+} \leftrightarrow Si_{TSi}^{4+}$
1→2	3.5	3.4	3.5
2→1	0.03	0.05	0.3
	$Si_{sp\langle 110 \rangle}^+$	$Si_{sp\langle 110 \rangle}^0$	$Si_{sp\langle 110 \rangle}^0$
	$\leftrightarrow Si_{sp\langle 110 \rangle}^+$	$\leftrightarrow Si_{sp\langle 110 \rangle}^0$	$\leftrightarrow Si_{sp\langle 1\bar{1}0 \rangle}^0$
1↔2	1.0	1.4	1.3

Fermi-levels below the mid-gap (by the large Madelung corrections $\varepsilon(3^+|4^+)$ is placed above the mid-gap). This is also consistent with our recent findings for Si_{TC} in 4H-SiC. The split-interstitial $Si_{sp\langle 110 \rangle}$ dominates in intrinsic and n-type material. It has several deep states within the band gap and is stable in the charge states 2^+ , 1^+ , and the neutral state. The ionization levels are given in Tab. I. For the diffusion in intrinsic and n-type material the neutral configuration is most important.

In p-type material all migration paths begin and end at the Si_{TC} site. The migration of Si_{TC} proceeds basically by two different mechanisms: (i) a kick-out mechanism via via the split-interstitials $Si_{sp\langle 100 \rangle}$ and $Si_{sp\langle 110 \rangle}$ as intermediate sites and (ii) a direct migration via a silicon coordinated interstitial site Si_{TSi} . In the kick-out mechanism the tetrahedral interstitial moves towards one of its silicon neighbors and forms a split-interstitial as an intermediate site as indicated in Fig. 2. To complete the migration, one of the silicon atoms of the split-interstitial moves to a neighboring Si_{TC} -site. The energy barriers for the migration via the different intermediate sites are listed in Tab. III. The lowest barrier is obtained for the migration via $Si_{sp\langle 110 \rangle}$. The barriers for the other paths are only slightly higher 0.1 eV. In case of the kick-out mechanism the transition state lies in the vicinity of the intermediate site, which is found to be hardly stable. For the direct path the intermediate Si_{TSi} is more stable with a barrier of 0.3 eV.

In intrinsic (compensated) and n-type material the interstitial migration of $Si_{sp\langle 110 \rangle}^0$ dominates. As indicated in Fig. 2c the migration proceeds by hops of one of the silicon atoms to the next silicon lattice site, where a new $Si_{sp\langle 110 \rangle}$ -interstitial is formed. A barrier of 1.4 eV is found for this hop. The interstitial may also change its orientation. For example, by the rotation of the pair around the (001)-axis the orientation changes from (110) to ($1\bar{1}0$). This process is associated with a barrier of 1.3 eV. We have also considered the positive interstitial, which migrates with a barrier of 1.0 eV.

So far the migration of interstitials has not been investigated on an *ab initio* level in 4H-SiC. However, our analysis of the ground state configurations shows⁴⁷ that the carbon split-interstitials at the carbon and silicon lattice

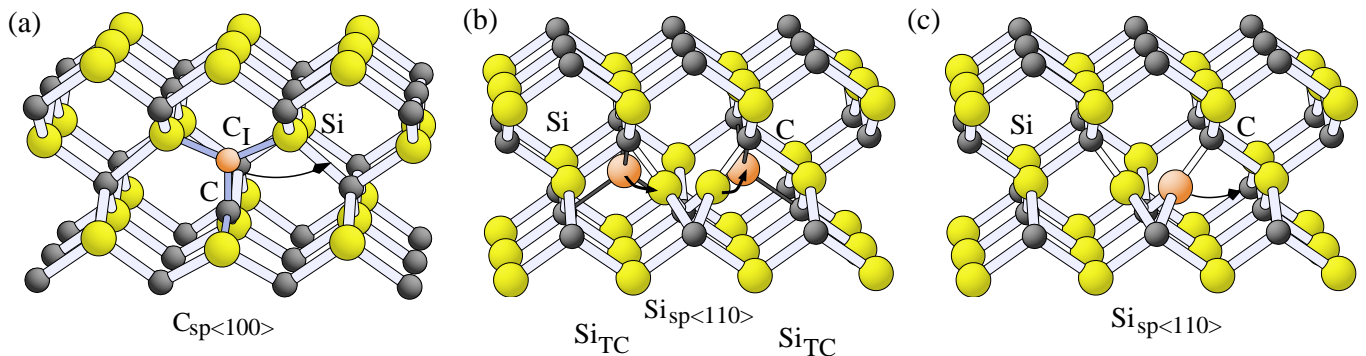


FIG. 2: Migration of interstitial: (a) migration of the carbon split-interstitial by second neighbor hops, (b) kick-out migration of the silicon interstitial between adjacent Si_{TC} -sites via the split-interstitial $\text{Si}_{\text{sp}<110>}$, and (c) migration of the silicon interstitial between adjacent $\text{Si}_{\text{sp}<110>}$ configurations.

sites have identical properties as in 3C-SiC, except that $\text{C}_{\text{sp}<100>}^{2-}$ becomes stable in n-type 4H-SiC. For the silicon interstitials in 4H-SiC, besides the sites discussed for 3C-SiC, additional sites appear: a site where the interstitial has simultaneously four carbon and silicon neighbors, and an open cage formed by the hexagonal rings of two adjacent lattice planes. For the interstitial sites with cubic environment we have found similar properties to 3C-SiC, also with respect to the (110)-oriented split-interstitial. In the open cage a position close to three carbon neighbors is preferred. The interstitial with four silicon and carbon neighbors is energetically unfavorable and may represent an intermediate site of a migration path. From the bonding properties of the interstitials we expect similar migration barriers as in 3C-SiC.

B. Vacancy migration

The ground state properties of the carbon and silicon vacancy have been discussed in detail by Zywiets *et al.*⁴⁸ and Torpo *et al.*⁴⁹. Here we briefly summarize a few facts for the sake of clarity. Both vacancies have a three-fold degenerate level within the band gap. Its occupation leads in case of the carbon vacancy (V_{C}) to a considerable Jahn-Teller-relaxation. The vacancy can exist in the charge states 2^+ , 1^+ , and neutral. Our calculation indicate that the negative charge states should not be realized. The ionization levels are listed in Tab. I. According to our calculations the positive charge state is unstable due to a negative-U behavior. However, for U , which is given by $U = \varepsilon(|+|++) - \varepsilon(0|+)$, we obtain a rather small value of -0.15 eV. This value should be considered as an estimate that depends on the size of the supercell and on the correction for the total energy of the charge defect.³⁷ Neglecting this correction, Zywiets *et al.*⁴⁸ arrived at $U = -0.48$ eV. In contrast to our findings, the calculations of Torpo *et al.*⁴⁹ suggest the absence of a negative-U behavior. However, the deviations in the results for U are within the uncertainty in the evaluation

of total energies for charged defects of about 0.2 eV. Irrespective whether a small negative-U is present or not, the positive charge state becomes relevant for μ_{F} around the ionization level $\varepsilon(0|++) = 1.2$ eV, in particular, when the Fermi level is pinned by an excess concentration of vacancies. This is also suggested by the recent identification of the EI5-center in 4H-SiC as a positive carbon vacancy,^{16,23} which shows a similar behavior as V_{C}^+ in 3C-SiC.

The DFT-LDA calculations predict that the silicon vacancy prefers a high-spin state over a Jahn-Teller-distorted ground state. This is consistent with the findings of spin-resonance experiments^{14,17} for V_{Si}^- . According to our analysis the silicon vacancy is realized in the charge states 1^+ , neutral, 1^- , and 2^- in 3C-SiC. Already in p-type material the vacancy becomes neutral and changes to a negative charge state for a Fermi-level at 0.6 eV. The charge state 2^- is stabilized in n-type material.

In 4H-SiC the carbon and silicon vacancy possess similar properties. The occupation of the lattice sites with local cubic and hexagonal coordination introduces negligible changes for the silicon vacancy. In case of V_{Si}^- the calculation of HF-tensors²⁴ and EPR-experiments¹⁴ show that the two sites cannot be distinguished. Also for the carbon vacancy similar formation energies and ionization levels are obtained at the cubic and hexagonal site. However, the different rehybridisation of the silicon dangling bonds²⁴ affects the local symmetry and for V_{C}^+ leads to different HF-signatures at the cubic and hexagonal sites.²⁴ A relevant effect for the diffusion in n-type 4H-SiC is the stabilization of additional negative charge states (V_{C}^- , V_{C}^{2-} , V_{Si}^{3-} , and V_{Si}^{4-}) due to the larger band gap.

For the migration of the vacancies we have analyzed mechanisms that involve either nearest neighbor hops or second neighbor hops. In Fig. 3 both mechanisms are indicated for the carbon vacancy. Our analysis has shown²³ that the silicon and carbon vacancies migrate by second neighbor hops.^{39,46} The arguments that rule out a migration entirely based on nearest neighbor hops are as fol-

lows. By a nearest neighbor hop the vacancy transforms into a vacancy-antisite-complex as the silicon (carbon) neighbor moves onto the sublattice of the opposite kind, thereby creating an antisite next to the vacant lattice site. In the case of the carbon vacancy we have found that the silicon vacancy-antisite-complex is unstable in all relevant charge states.²⁹ A barrier that could stabilize the vacancy-antisite complex is not present. This finding rules out any migration mechanism based on nearest neighbor hops for the carbon vacancy. In case of the silicon vacancy, it has been found by us²⁹ in 3C-SiC and by Rauls *et al.*²⁸ for the neutral complex in 4H-SiC that the carbon vacancy-antisite-complex may be more stable than the vacancy. This metastability of the silicon vacancy occurs in p-type and intrinsic (compensated) material and has implications on the migration as well as the annealing of V_{Si} . It will be considered in detail in Sec. III C. However, a migration mechanism entirely based on nearest neighbor hops is impossible: a consecutive nearest neighbor hop would transform the $V_{\text{C}}\text{-C}_{\text{Si}}$ -complex into a $V_{\text{Si}}\text{-Si}_{\text{C}}\text{-C}_{\text{Si}}$ -complex. We have found that this complex is unstable.

Our analysis of the second neighbor hop, its migration path and the calculation of the migration barriers is discussed in detail in Ref. 39. Here we basically summarize our findings for the migration barriers as tabulated in Tab IV. The barriers are obtained using the 216 atom cell and the Γ -point for the k-summation. This also allowed for the proper inclusion of Jahn-Teller distortions in case of the carbon vacancy and the inclusion of spin polarization for the silicon vacancy. Using a 64 atom cell and special k-points ($2 \times 2 \times 2$ Monkhorst-Pack mesh) the calculated barriers agree within 0.3 eV. For the carbon vacancy we find relatively high migration barriers. They strongly depend on the charge state and vary between 5 eV in p-type material (V_{C}^{2+}) and 3.5 eV in n-type material (V_{C}^0). The charge state dependence has its origin in the successive occupation of bonding defect levels at the transition state. For the silicon vacancy we obtain smaller migration barriers and a less pronounced dependence on the charge state. The migration barrier in p-type and intrinsic material with values between 3.2 eV and 3.6 eV is larger than the barrier for the transformation into the carbon vacancy-antisite-complex. The implications of this finding are discussed in the next section. In n-type material the migration barrier amounts to 2.4 eV (V_{Si}^{2-}). Since the vacancy is stable in n-type material, a possible transformation of the vacancy here does not interfere with its migration.

C. Metastability of the silicon vacancy

Our results in 3C- and 4H-SiC for the metastability of the silicon vacancy (in 4H-SiC we have considered complexes with the vacancy-antisite pair located at neighboring cubic or hexagonal sites and aligned along the c -axis) and the findings of Lingner *et al.*²⁶ suggest that the follow-

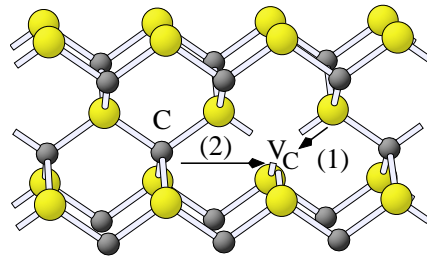


FIG. 3: Migration of the carbon vacancy: (1) nearest neighbor hop (2) migration on the carbon sublattice by second neighbor hops.

TABLE IV: Vacancy migration and transformation of V_{Si} into $V_{\text{C}}\text{-C}_{\text{Si}}$: Energy barriers for the relevant charge states.

path	energy barriers [eV]				
	2^+	1^+	0	1^-	2^-
$V_{\text{C}} \rightarrow V_{\text{C}}$	5.2	4.1	3.5	-	-
$V_{\text{Si}} \rightarrow V_{\text{Si}}$	-	3.6	3.4	3.2	2.4
$V_{\text{Si}} \rightarrow V_{\text{C}}\text{-C}_{\text{Si}}$	-	1.9	2.4 (2.2)	2.5	2.7
$V_{\text{C}}\text{-C}_{\text{Si}} \rightarrow V_{\text{Si}}$	6.1	4.2	3.5 (2.4)	2.4	-

ing discussion is not restricted to a certain polytype. The silicon vacancy and the carbon vacancy-antisite-complex may be transformed into each another by a nearest neighbor hop as discussed above. Depending on the doping conditions a metastability of the silicon vacancy arises, when the $V_{\text{C}}\text{-C}_{\text{Si}}$ -complex is more stable than the silicon vacancy. This is the case in p-type and intrinsic (compensated) material. A stable silicon vacancy is retained for a Fermi-level position above 1.7 eV. This is demonstrated in Fig. 4. For a given Fermi-level, the two defects V_{Si} and $V_{\text{C}}\text{-C}_{\text{Si}}$ possess different charge states, as the transformation of V_{Si} into $V_{\text{C}}\text{-C}_{\text{Si}}$ rises the position of localized states within the band gap.

The energy barriers we have obtained for the transformation $V_{\text{Si}} \rightarrow (V_{\text{C}}\text{-C}_{\text{Si}})$ and the reverse process $(V_{\text{C}}\text{-C}_{\text{Si}}) \rightarrow V_{\text{Si}}$ are listed in Tab. IV. The values refer to our recent results obtained for 3C-SiC using a 216 atom cell and the Γ -point and include spin effects.³⁹ The barriers are calculated for each given charge state. We assume that the initial charge state is preserved during the transformation and equilibrates at the final configuration. This applies also to the transformation of $V_{\text{Si}}^{2-} \rightarrow (V_{\text{C}}\text{-C}_{\text{Si}})^{2-}$ and $(V_{\text{C}}\text{-C}_{\text{Si}})^{2+} \rightarrow V_{\text{Si}}^{2+}$, where the final configurations $(V_{\text{C}}\text{-C}_{\text{Si}})^-$ and V_{Si}^+ are the ground state configurations. For all charge states the transformation occurs in a low-spin state, except for V_{Si}^0 where the high-spin state has a lower barrier (given in braces in Tab. IV). Since this high-spin state is not the ground state of the final $V_{\text{C}}\text{-C}_{\text{Si}}$ -complex, the complex relaxes into the low-spin state before a reverse transformation occurs.

The metastability of the vacancy in p-type and its

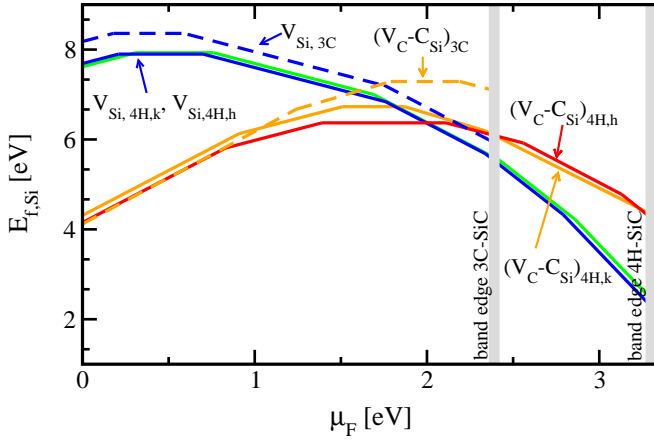


FIG. 4: Formation energy of the silicon vacancy V_{Si} and the carbon vacancy-antisite-complex $V_{\text{C}}\text{-C}_{\text{Si}}$ for 3C-SiC and 4H-SiC. The experimental band edges of 3C- and 4H-SiC are indicated by vertical bars. The subscripts refer to the polytype and the cubic and hexagonal lattice site (k and h respectively). $(V_{\text{C}}\text{-C}_{\text{Si}})_{4\text{H},k}$ and $(V_{\text{C}}\text{-C}_{\text{Si}})_{4\text{H},h}$ refer to complexes with the vacancy and antisite at either cubic or hexagonal sites that are aligned along the c-axis.

stabilization in n-type material is accompanied with a pronounced variation of the transformation barriers with the charge state. In p-type material the transformation $V_{\text{Si}} \rightarrow V_{\text{C}}\text{-C}_{\text{Si}}$ has a much lower barrier with values between 1.9 and 2.5 eV than the reverse transformation with a barrier between 6.1 eV and 3.5 eV. The transformation is thus more likely than the reverse transformation. Only when $(V_{\text{C}}\text{-C}_{\text{Si}})^-$ becomes stable, i.e. in n-type 3C-SiC, the transformation of V_{Si}^{2-} has a lower probability than the transformation of $(V_{\text{C}}\text{-C}_{\text{Si}})^-$.

A comparison of the transformation barrier with the migration barrier shows that the transformation occurs with a much higher probability than the migration in the charge states 1^+ , neutral and 1^- , which are relevant in p-type and compensated material. The reverse transformation $V_{\text{C}}\text{-C}_{\text{Si}} \rightarrow V_{\text{Si}}$ has much larger barriers than the migration of V_{Si} . Note that the relevant charge states are 2^+ and 1^+ for this process in p-type material. Therefore, the vacancy migration is kinetically hindered for low and moderate temperatures unless the reverse transformation is activated at high temperatures. Then a migration of $V_{\text{C}}\text{-C}_{\text{Si}}$ may take place via V_{Si} . The effective barrier for the migration path $V_{\text{C}}\text{-C}_{\text{Si}} \rightarrow V_{\text{Si}} \rightarrow V_{\text{Si}} \rightarrow (V_{\text{C}}\text{-C}_{\text{Si}})$ is given by the formation energies $E_{\text{f}}^{V_{\text{Si}}}$, its migration barrier $E_{\text{m}}^{V_{\text{Si}}}$, and the formation energy $E_{\text{f}}^{V_{\text{C}}\text{-C}_{\text{Si}}}$ of the complex

$$E_{\text{m,eff}} = E_{\text{f}}^{V_{\text{Si}}} - E_{\text{f}}^{V_{\text{C}}\text{-C}_{\text{Si}}} + E_{\text{m}}^{V_{\text{Si}}} \quad (4)$$

In p-type material this effective barrier amounts to 7.7 eV and drops to a value of 4.3 eV for $\mu_{\text{F}} = 1.2$ eV around mid-gap, when the vacancy is negative. The effective barrier is still 3.2 eV at $\mu_{\text{F}} = 1.76$ eV, when the silicon vacancy becomes doubly negative. Here we have assumed

TABLE V: Recombination of vacancies and interstitials: Energy barriers of Frenkel pairs for the relevant charge states. The geometry of the Frenkel pairs is displayed in Fig.5.

Frenkel pair	energy barriers [eV]		
	2^+	1^+	0
$\text{C}_{\text{sp}\langle 100 \rangle}\text{-V}_{\text{C}}$	1.0	0.5	0.4
$\text{C}_{\text{spSi}\langle 100 \rangle}\text{-V}_{\text{C}}$	1.2	1.2	1.4
$\text{Si}_{\text{sp}\langle 110 \rangle}\text{-V}_{\text{Si}}$	0.0	~ 0.2	0.2

that the charge state equilibrates at the vacancy. If this is not the case, the effective migration barrier for the positive and neutral $V_{\text{C}}\text{-C}_{\text{Si}}$ -complexes are 6.3 eV and 4.5 eV respectively.

Besides a migration of a metastable silicon vacancy, also a dissociation of the carbon vacancy-antisite-complex has to be considered.⁴⁶ In this case the carbon vacancy migrates away from the antisite at the expense of the binding energy. Using the migration barrier for V_{C} between 3.5 eV (V_{C}^0) to 5 eV (V_{C}^{2+}) plus the binding energy of about 1 eV as an estimate for the dissociation barrier, we obtain values of 6.2 eV for $(V_{\text{C}}\text{-C}_{\text{Si}})^{2+}$ and 4.5 eV for $(V_{\text{C}}\text{-C}_{\text{Si}})^0$. Only in p-type material this process has a similar probability as the reverse transformation followed by a migration of the silicon vacancy.

We have not investigated the transformation barriers in 4H-SiC. Rauls *et al.*²⁸ have obtained a transformation barrier of 1.7 eV for the neutral vacancy using a DFT-based tight-binding scheme, which is in agreement with our results. Therefore we expect a similar charge state dependence of the barriers in 4H-SiC as discussed above. For the charge states 3^- and 4^- of the vacancy we expect larger barriers for the transformation $V_{\text{Si}} \rightarrow (V_{\text{C}}\text{-C}_{\text{Si}})$ and correspondingly lower barriers for the reverse transformation.

IV. RECOMBINATION OF FRENKEL PAIRS

A. Carbon vacancies

In a carbon Frenkel pair the interstitial and vacancy may be nearest neighbors or second neighbors. Also vacancies and interstitials may attract each other over larger distances. For their recombination the interstitial has to migrate to the vacancy. In the following we analyze the recombination of Frenkel pairs where a carbon split-interstitial is a nearest or second neighbor of the carbon vacancy.

The nearest-neighbor-pair $\text{C}_{\text{spSi}\langle 100 \rangle}\text{-V}_{\text{C}}$ is a vacancy-complex with a carbon split-interstitial at the silicon site. Two different configurations are possible: a stable configuration with a threefold coordinated carbon interstitial and a silicon dangling bond as depicted in Fig 5a, and another configuration in which the carbon interstitial possesses one carbon neighbor. This latter pair turned

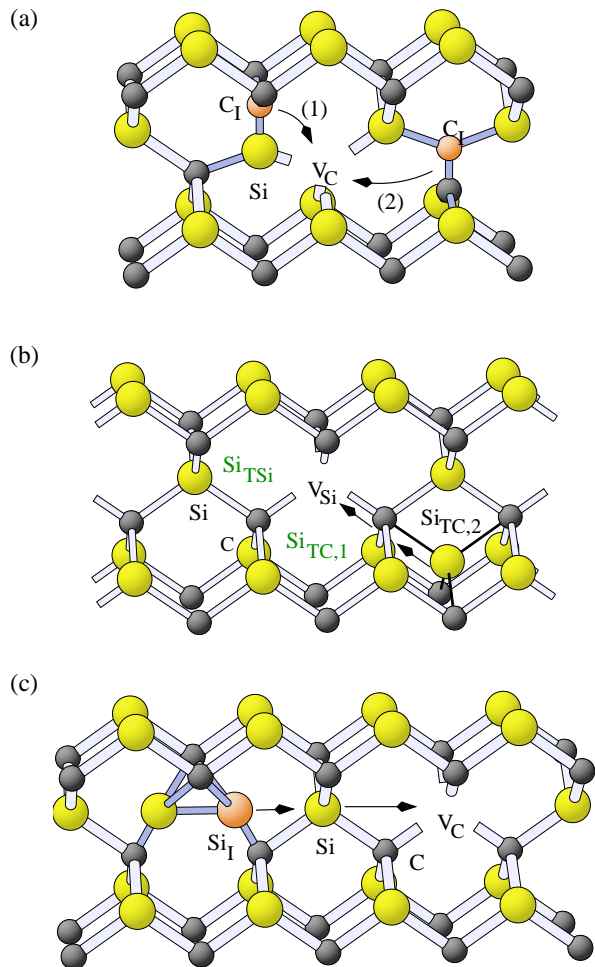


FIG. 5: Recombination of carbon and silicon Frenkel pairs: (a) carbon nearest-neighbor-pair $C_{\text{spSi}(100)}-V_{\text{C}}$ and second-neighbor pair $C_{\text{sp}(100)}-V_{\text{C}}$, (b) silicon Frenkel pairs with Si_{TC} -interstitial (the labels Si_{TSi} and $\text{Si}_{\text{TC},1}$ indicate the unstable sites) and (c) fourth-neighbor-pair $\text{Si}_{\text{sp}(110)}-V_{\text{Si}}$. The lowest energetic path of the interstitial atom is indicated by arrows.

out to be unstable. The first configuration exists in the charge states 2^+ through 1^- with the ionization levels at 0.4 eV ($+|2+$), 0.7 eV ($0|+$), and 1.8 eV ($-|0$). The defect states are formed by a silicon p -orbital of the interstitial and the dangling bond of the vacancy within the same plane. Using the saddle point search method and a 64 atom cell with special k -points we have obtained a recombination barrier for the neutral charge state of 1.4 eV (c.f. Tab. V). At the transition state the occupied defect levels are well localized. Towards the end of the recombination they transform into delocalized valence band states. The pair may also recombine in the positive charge states. There we expect the neutralization by an electron transfer at the end of the recombination. In this case a recombination barrier can be calculated and we obtain 1.2 eV for $(C_{\text{spSi}(100)}-V_{\text{C}})^{2+}$ and $(C_{\text{spSi}(100)}-V_{\text{C}})^{1+}$. For $(C_{\text{spSi}(100)}-V_{\text{C}})^-$, which is relevant in n -type material, a second defect level is occupied

that transforms into a delocalized conduction band state during the recombination. Two possibilities exist in this case: firstly, the defect is converted to neutral by an electron transfer before the recombination or secondly, in the final stage of the recombination the additional electron is donated into the conduction band. The treatment of both cases is beyond the scope of the present work.

In the second-neighbor-pair $C_{\text{sp}(100)}-V_{\text{C}}$ the interstitial is located at the neighboring carbon site, as depicted in Fig. 5a. The pair exists in the charge states 2^+ , 1^+ , 0 and 1^- , with the ionization levels $\varepsilon(+|2+)=0.8$ eV, $\varepsilon(0|+)=1.1$ eV and $\varepsilon(-|0)=1.6$ eV. The defect states mainly derive from the interstitials levels. The recombination occurs by a second-neighbor hop of the upper carbon atom via the unstable $C_{\text{spSi}(100)}$ -configuration as indicated in Fig. 5a. The recombination barriers for the pair are listed in Tab. V. With values between 1.0 eV and 0.4 eV they are considerably lower than the barriers for the recombination of $C_{\text{spSi}(100)}-V_{\text{C}}$. The barrier is also lower than the migration barrier of the split-interstitials. For the negative charge state a similar mechanism as for the negative nearest-neighbor pair has to be considered.

In p -type material the vacancy and the approaching interstitial may be positively charged. An additional long range Coulomb repulsion may hinder the recombination. The barrier for the formation of the Frenkel pair is then given by the migration barrier of the interstitial plus the Coulomb repulsion of the pair. On the other hand, once the defect levels begin to overlap new states are formed. The charge state will be successively reduced by electron transfer to the defect levels. Indeed, for the Frenkel pairs discussed above the total charge of the isolated defects $C_{\text{sp}(100)}^{2+}$ and V_{C}^{2+} is reduced to 2^+ or 1^+ .

A considerable energy gain is associated with the formation of the Frenkel pairs $C_{\text{spSi}(100)}-V_{\text{C}}$ and $C_{\text{sp}(100)}-V_{\text{C}}$ from the isolated defects $C_{\text{sp}(100)}$ and V_{C} . The binding energy for $C_{\text{spSi}(100)}-V_{\text{C}}$ varies between 2 eV for $(C_{\text{spSi}(100)}-V_{\text{C}})^{2+} \rightarrow C_{\text{sp}(100)}^0 + V_{\text{C}}^{2+}$ and 4 eV for $(C_{\text{spSi}(100)}-V_{\text{C}})^0 \rightarrow C_{\text{sp}(100)}^0 + V_{\text{C}}^0$. For the second-neighbor pair $C_{\text{sp}(100)}-V_{\text{C}}$ we obtain values between 0.8 eV for $(C_{\text{sp}(100)}-V_{\text{C}})^{2+} \rightarrow C_{\text{sp}(100)}^0 + V_{\text{C}}^{2+}$ and 1.0 eV for the separation of the neutral pair. The interstitial is thus attracted by the vacancy once the charge state has equilibrated.

Recently, the recombination of vacancies with carbon split-interstitials was investigated in 4H-SiC using a DFT-based tight-binding scheme.⁵⁰ Only neutral Frenkel pairs were considered. A similar recombination barrier of the neutral pair $C_{\text{sp}(100)}-V_{\text{C}}$ (0.5 eV) was found as in our calculation for 3C-SiC. Larger barriers were obtained for the direct recombination of more remote pairs.

B. Silicon vacancies

Frenkel pairs involving the silicon vacancy may be formed with either of the dominant interstitials Si_{TC} ,

$\text{Si}_{\text{sp}(110)}$ and with the silicon-coordinated interstitial Si_{TSi} . The Frenkel pairs with Si_{TC} and Si_{TSi} should account for the recombination in p-type material, when the Si_{TC} -site is relevant for the migration. A recombination via the Frenkel pair with $\text{Si}_{\text{sp}(110)}$ should be relevant in intrinsic (compensated) and n-type material, where split-interstitials dominate.

First we have analyzed Frenkel pairs formed with a Si_{TSi} - or Si_{TC} -interstitial neighboring the silicon vacancy. The Frenkel pairs with a Si_{TC} -interstitial or a Si_{TSi} -interstitial next to the vacancy turned out to be unstable in all relevant charge states (the labels $\text{Si}_{\text{TC},1}$ and Si_{TSi} indicate the sites of the interstitial in Fig. 5b). Upon reaching these sites, the interstitial immediately recombines with the vacancy. The closest stable Frenkel pair we found involves an interstitial at a Si_{TC} -site with only one common carbon neighbor to the vacancy (c.f. the $\text{Si}_{\text{TC},2}$ -site in Fig. 5b). This stable Frenkel pair has deep levels within the band gap. It is only realized in the positive and neutral charge state with ionization levels at $\varepsilon(+|2+) = 0.5\text{ eV}$ and $\varepsilon(0|+) = 1.2\text{ eV}$. The recombination of this pair could be achieved via a hop of the interstitial passing close by the adjacent Si_{TSi} -site. Our calculations indicate that this is not a likely path. Instead an anti-structure pair forms by a hop of the carbon neighbor into the silicon vacancy. In a concerted motion the interstitial moves into the site left by the carbon neighbor. The reaction barrier amounts to 3.2 eV for the positive and the neutral Frenkel pair, which is comparable with the migration barrier of Si_{TC} .

Frenkel pairs with the split-interstitial $\text{Si}_{\text{sp}(110)}$ represent other possible configurations. It turns out that $\text{Si}_{\text{sp}(110)}\text{-V}_{\text{Si}}$ is unstable when the vacancy and the interstitial are second neighbors, irrespective of the orientation of the pair. A recombination barrier thus may be encountered for more distant pairs, e.g. with the interstitial at the third or fourth neighbor shell. The recombination of such pairs is based on the migration of the split interstitial to an unstable second neighbor position. Here we discuss the fourth-neighbor Frenkel pair in more detail. Our findings for this pair suggest a similar mechanism for the third neighbor pair. The fourth-neighbor complex is stable except in highly doped p-type material. In the doubly positive charge state the interstitial and the vacancy immediately recombine. The complex becomes positively charged at the ionization levels ($2^+|1^+$)=0.48 eV. For a Fermi level above mid-gap the complex is neutral or negative (ionization levels: ($1^+|0$)=1.3 eV and ($0|1^-$)=1.8 eV). It is doubly negative in strongly doped n-type material only (ionization level($2^-|1^-$)=2.3 eV). The saddle point search finds the following recombination mechanism (c.f. Fig. 5c): first the silicon interstitial jumps towards the silicon-neighbor it has in common with the vacancy, then this neighbor is kicked out of its site and recombines with the vacancy. This process is accompanied with a barrier of 0.2 eV. As the split-interstitial close to the vacancy is unstable, the barrier for this process is considerably lower than the

TABLE VI: Dissociation energy of neutral interstitial and vacancy clusters. For the interstitial clusters the given value is the energy needed to remove a single carbon atom.

Polytype	Cluster	Dissociation energy (eV)
3C	$(\text{C}_{\text{sp}})_2$	2.8
3C	$(\text{C}_{\text{sp}})_3$	3.0
3C	$(\text{C}_{\text{sp}})_4$	5.7
4H	$(\text{C}_{\text{sp}})_{2,\text{kh}}$	5.8
4H	$(\text{C}_{\text{sp}})_{2,\text{hh}}$	5.0
4H	$(\text{C}_{\text{sp}})_{2,\text{kk}}$	4.6
3C	$\text{V}_{\text{C}}\text{-V}_{\text{Si}}$	4.5
3C	$\text{V}_{\text{C}}\text{-V}_{\text{C}}$	1.7
3C	$\text{V}_{\text{Si}}\text{-V}_{\text{Si}}$	0.1

TABLE VII: Ionization levels of the investigated interstitial clusters. The tri-interstitial $(\text{C}_{\text{sp}})_3$ exhibits a negative- U effect for the positive charge states and the tetra-interstitial $(\text{C}_{\text{sp}})_4$ is electrically inactive.

		$\varepsilon(1^+ 2^+)$	$\varepsilon(0 1^+)$	$\varepsilon(1^- 0)$	$\varepsilon(2^- 1^-)$
3C	$(\text{C}_{\text{sp}})_2$	0.8	0.99	-	-
3C	$(\text{C}_{\text{sp}})_3$	0.85	0.62	1.49	1.8
3C	$(\text{C}_{\text{sp}})_4$	-	-	-	-
4H	$(\text{C}_{\text{sp}})_{2,\text{kh}}$	-	0.10	2.78	3.13
4H	$(\text{C}_{\text{sp}})_{2,\text{hh}}$	0.41	0.50	2.82	2.68
4H	$(\text{C}_{\text{sp}})_{2,\text{kk}}$	0.32	0.38	2.66	2.6

barrier for the interstitial migration. As discussed for the annealing of carbon vacancies, we expect a higher barrier for the recombination in the negative charge state of the complex.

Thus the analysis of the silicon Frenkel pairs shows that the pairs with a short distance between the interstitial and the vacancy are unstable, except for the second neighbor pair pair $\text{V}_{\text{Si}}\text{-Si}_{\text{TC},2}$. For the stable pairs we have found recombination barriers that are somewhat lower than the migration barriers of the interstitial. These findings suggest a recombination based on a migration towards the closest stable sites. They also indicate that the energy barriers of this process should not exceed the migration barrier of the corresponding interstitial.

V. CLUSTERING OF CARBON INTERSTITIALS

A formation of composite defects, e.g. D_{I} or D_{II} centers, during annealing requires a reservoir of intrinsic defects. However, at elevated temperatures vacancies and interstitials anneal out. (see discussion in Sec. VI). Yet, the point defects can be kinetically supplied by defect precipitations. The clusters of vacancies and interstitials can then serve as sources of mobile defects. We expect

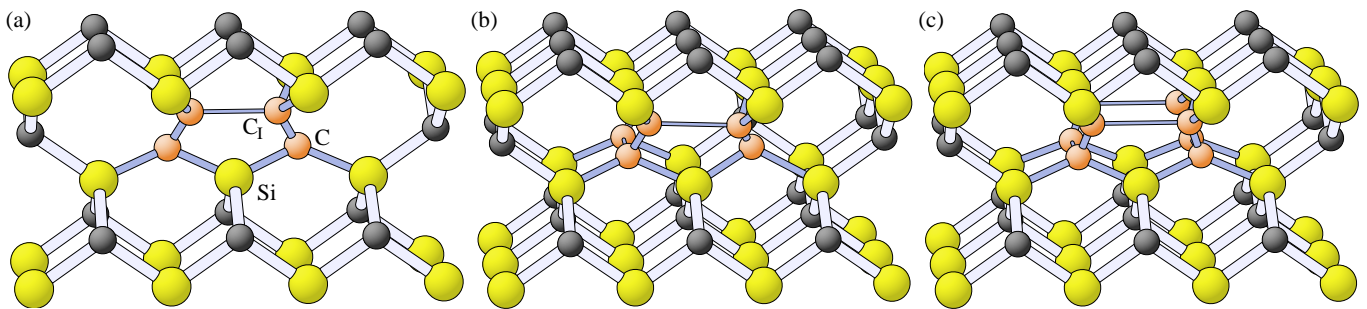


FIG. 6: Carbon interstitial clusters in 3C-SiC: (a) Di-interstitial (C_{sp}^2) (b) Tri-interstitial (C_{sp}^3) (c) Tetra-interstitial (C_{sp}^4)

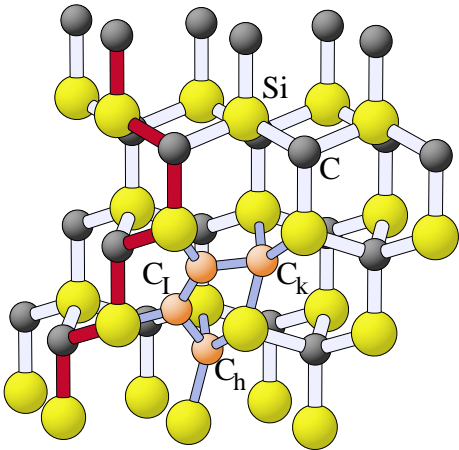


FIG. 7: Di-interstitial (C_{sp}^2)_{kh} in 4H-SiC located on a cubic and a hexagonal site. The subscripts k and h refer to cubic and hexagonal sites. C_1 refers to the additional carbon atoms. The stacking sequence of the crystal is indicated by the dark bonds.

that the effect of the interstitial clusters on the defect kinetics is much more pronounced than that of the vacancy clusters. Although both cluster types possess sizeable dissociation energies (cf. Tab. VI and Ref. 51 for the divacancy), the migration barriers of the carbon and the silicon vacancies are much higher than those of the interstitials (cf. Sec. III) so that it is much more likely that the interstitials combine into precipitates. In addition, we expect (cf. Sec. VI) that the vacancy-interstitial recombination sets in before a significant vacancy clustering occurs.

We focus in this section on small clusters formed by upto four carbon interstitials. Due to the high mobility of the carbon interstitials, these clusters may act as a sink for interstitials at lower temperatures and can reemit them at higher temperatures. Similar aggregates have already been investigated in diamond.⁵² The microscopic structure of the considered complexes is displayed in Fig. 6 for 3C-SiC, an example of the di-interstitial in 4H-SiC is shown in Fig. 7. A detailed analysis of the electronic structure and the vibrational spectra is given elsewhere.⁵³ Here we summarize the facts that are im-

portant for the annealing mechanisms. The focus is on the dissociation energies of these defects, i.e. the energy needed to remove a single carbon atom from these clusters. For a mid-gap Fermi-level all clusters are neutral. The results for the dissociation energy in the neutral charge state are listed in Tab. VI.

The carbon split-interstitial possesses two dangling p -orbitals oriented in (110) -direction, resulting from the sp^2 -hybridization of the carbon atoms. The two adjacent split-interstitials form a covalent bond due to the overlap of these orbitals. This (cf. Fig. 6a) results in a more favorable sp^3 -hybridization of the two interstitial carbon atoms and gives rise to an energy gain of 2.8 eV for the carbon di-interstitial (C_{sp}^2). In the same way further carbon atoms can be absorbed, resulting in larger carbon aggregates. The tri-interstitial (Fig. 6b) possesses a similar dissociation energy (3.0 eV) as the di-interstitial. In the tetra-interstitial a ring of split-interstitials is formed (Fig. 6c) which is especially favorable. All carbon atoms are sp^3 -hybrids, hence all bonds are saturated. This leads to an energy gain of 5.7 eV for the added carbon interstitial.

The charge states of the investigated clusters are listed in Tab. VII. The di-interstitial possesses all charge states from 2+ to 0. The tri-interstitial is mainly neutral, only at the band edges the charge states 2+ and 2- can exist. This cluster exhibits a negative- U effect, since it is energetically favorable to fully occupy the connecting bonds between all three adjacent split-interstitials (cf. Fig. 6b). The tetra-interstitial is electrically inactive, since all carbon p -orbitals are saturated.

In 4H-SiC, a stronger relaxation and rehybridization of the carbon atoms is observed than in 3C-SiC. Therefore already the di-interstitial shows a very high stability. Three different variations of the di-interstitial are possible. The split-interstitials can either lie completely in a hexagonal or a cubic plane, or they occupy two adjacent cubic and hexagonal sites (cf. Fig. 7). With a binding energy of 5.8 eV the latter is the most stable configuration. This higher binding energy compared to 3C-SiC results from the sp^3 -hybridization of the border atoms, which is preferred due to the different geometry of the hexagonal planes in 4H-SiC. Also the hexagonal and cubic di-interstitials are very stable with binding energies

of 5.0 eV and 4.6 eV, respectively. These di-interstitials show a strong distortion and have a nearly linear structure within their cubic or hexagonal plane.

The micro-clusters presented in this section are examples of clustering processes. The formation of cluster networks via bonds between the p-orbitals of adjacent $(C_{sp})_2$ and $(C_{sp})_3$ clusters is also possible. Additionally, carbon antisites can trap carbon interstitials with sizable binding energies.⁴⁶ In the discussion of the annealing mechanisms below we outline the competition of the cluster formation with the vacancy-interstitial recombination and their role as a source for carbon interstitials at the high temperature annealing stages.

VI. HIERARCHY OF ANNEALING MECHANISMS

The annealing of vacancies and interstitials is governed by several competing mechanisms. The principal mechanisms are (i) the recombination of vacancies and interstitials, (ii) the out-diffusion to the surface, (iii) the diffusion to sinks, where they are annihilated or otherwise form stable complexes, and (iv) the transformation into other more stable configurations that is not diffusion-related. Sinks for interstitials or vacancies could be immobile defects, such as interstitial clusters and stable complexes with impurities, or extended defects, such as dislocations. In the latter cases the interstitial or vacancy are not disappearing as such, but are bound in a more stable form. In the experiment, nevertheless, the observed signatures *anneal out*, while other centers related to the annealing may appear in the spectra.

The experimental investigation of the annealing kinetics requires a sufficient temperature T to activate one or more of the above annealing mechanisms. The diffusion-limited mechanisms (ii)-(iii) and the transformation-related mechanisms are typically described by first order kinetics with an activation energy given by the migration or transformation barrier (e.g. Ref. 54). The kinetics of the vacancy-interstitial recombination depends on the average separation of the vacancy and interstitial. For bound Frenkel pairs the activation energy is given by the recombination barrier. For uncorrelated vacancy-interstitial pairs (e.g. when their separation is much larger than the capture radius) the interstitial has to migrate to the vacancy (the vacancies are rather immobile) to form a Frenkel pair. The Frenkel pair then simply recombines by a hop of the interstitial into the vacant lattice site. In this case, as the recombination barriers of the Frenkel pair are found to be relatively small, the recombination is essentially limited by the diffusion of the interstitial. The recombination then is described by the activation energy of the interstitial migration. The prefactors of the diffusion-limited mechanisms and the vacancy-interstitial recombination, however, depend on parameters arising from the sample preparation, e.g. the average distribution (and concentration) of the defects

(and sinks), as well as the mutual interaction between the involved partners. Hence, the predictive translation of activation energies into annealing temperatures hinges on parameters that are specific to the particular samples. Only by detailed simulations it is possible to assess the initial state of the samples (e.g. after irradiation) and the annealing kinetics quantitatively. Our analysis forms the basis for such simulations, that are well beyond the scope of the present paper. Nevertheless, a qualitative assessment of the kinetics via the calculated activation energies should be valid, since the activation energies differ substantially in value and enter the rate constants exponentially.

In the following we deduce a hierarchy of annealing mechanisms based on a comparison of the energy barriers involved in the principal annealing mechanisms. Central to the discussion are four important observations. Our results for the migration of intrinsic point defects show that the interstitials are by far more mobile than the vacancies, also the recombination barriers for Frenkel pairs are lower than the migration barriers of the vacancies. The silicon vacancy is a metastable defect in p-type and compensated material. The migration of defects strongly depends on the charge state, in particular the migration of silicon interstitials and vacancies.

A. Silicon vacancies and interstitials

Qualitatively, the annealing of silicon vacancies is subject to three different Fermi-level dependent mechanisms: (i) the transformation of the silicon vacancy into a carbon vacancy-antisite complex, (ii) the Frenkel pair recombination with silicon split-interstitials and (iii) the migration of silicon vacancies to sinks. These mechanisms are summarized in Fig. 1.

In p-type material, we expect a dominance of the annealing of the vacancy signature by its transformation into the vacancy-antisite complex. The recombination of the stable Frenkel pairs, i.e. pairs with the Si_{TC} -interstitial located in the second neighbor shell or beyond, is suppressed by the larger migration/recombination barrier (3.2 eV-3.5 eV) as compared to the barrier of the transformation (1.9 eV-2.4 eV). Also the migration of the silicon vacancy is kinetically suppressed in p-type material due to the larger migration barrier (3.6 eV-3.2 eV). Once the silicon vacancy is transformed into the vacancy-antisite complex, it stays in this configuration. The reverse transformation requires fairly high temperatures due to the large barrier of 6.5 eV. As discussed in Sec. III C, the dissociation of the vacancy-antisite complex becomes possible at the same time.

In compensated material (with the Fermi level at or above mid-gap), the silicon split-interstitial is the most relevant interstitial configuration. Its migration barrier is lower than the transformation barrier of the silicon vacancy. Hence the vacancy-interstitial recombination prevails in the annealing hierarchy. For the recombina-

tion of bound Frenkel pairs we found a low barrier of 0.2 eV. The annihilation of vacancies by more distant interstitials is limited by the migration of the interstitial towards the vacancy with a migration barrier of 1.4 eV. It constitutes a separate annealing stage. Note that the small binding energy of the Frenkel pair indicates a weak attractive interaction between the interstitial and the vacancy. Hence a dissociation of distant pairs has a relatively high probability, which enables further annealing stages. The metastability-induced annealing is the next annealing stage in the hierarchy. As a final stage, the vacancy-antisite complex, that evolves from the silicon vacancy, anneals by dissociation or by its migration to sinks. Again the migration of silicon vacancies does not directly contribute as the migration barrier of 3.2 eV to 3.4 eV (V_{Si}^- and V_{Si}^0 respectively) is larger than the transformation barrier.

In n-type material the silicon vacancy becomes a stable defect. As in intrinsic (compensated) material the annealing by vacancy-interstitial recombination has a lower activation barriers than the vacancy migration. The migration of silicon vacancies to sinks is most likely the last stage in the hierarchy. It has a slightly higher barrier than the transformation $V_{\text{Si}} \rightarrow V_{\text{C-C}_{\text{Si}}}$ in compensated material.

By electron spin resonance experiments Itoh *et al.*¹⁷ observed the annealing of the T1-center in p-type and n-type 3C-SiC irradiated by electrons and protons. They found three annealing stages at 150°C, 350°C and 750°C. The annealing behavior was found to be insensitive to the doping (aluminum and nitrogen) and the irradiating particles (electrons and protons), except for the p-type electron-irradiated sample, where the final annealing occurred at 350°C in coincidence with the annealing of three other defect-centers. Itoh *et al.* argued that a possible loss of the paramagnetic state might be correlated with the annealing of two unidentified centers T6 and T7 that were only observed under these conditions.¹⁷ The independence of the annealing behavior of the particular dopants indicates that the observed annealing process itself involves only intrinsic defects.

The T1-center was identified by the authors as a negative silicon vacancy V_{Si}^- . Later this identification was verified theoretically^{14,22,23,39} by calculations of the hyperfine tensors. According to earlier theoretical results^{14,48,49} and our calculations (c.f. Tab. I) the silicon vacancy is in a negative charge state over a wide range of the Fermi level starting below mid-gap ($\mu_{\text{F}} > 0.6$ eV) and ending somewhat below the conduction band edge ($\mu_{\text{F}} < 1.76$ eV). This suggest that the p-type and n-type samples were compensated by the irradiation, most likely the Fermi level was trapped by irradiation-induced deep defects around mid gap. Under these conditions the scenario for compensated material we described above should explain the annealing of the EPR-signature of V_{Si}^- by three annealing stages, namely: (i) the initial recombination of Frenkel pairs with a small separation between the vacancy and interstitial, (ii) the recombina-

tion of vacancies and interstitials with a larger separation that is limited by the diffusion of the interstitial, and (iii) the transformation of V_{Si}^- into a carbon vacancy-antisite complex.

From the annealing experiments Itoh *et al.*⁵⁵ deduced an activation energy of 2.2 eV for the last annealing stage. According to our calculations the transformation of V_{Si}^- into $V_{\text{C-C}_{\text{Si}}}$, that constitutes the third annealing stage, is associated with an activation energy of 2.5 eV (c.f. Tab. IV) in good agreement with the experimental result. Once this transformation is activated silicon vacancies are largely transformed into carbon vacancy-antisite complexes and the EPR-signal of the T1-center vanishes. During the short observation times (5 min) of the isochronal annealing the reappearance of V_{Si}^- is kinetically hindered. Even though a signature of the carbon vacancy-antisite complex may develop in the spectra, Itoh *et al.* reportedly have not observed the appearance of a new defect center that could evolve from the silicon vacancy. Note, that for a Fermi level below 1.24 eV the vacancy-antisite complex is not paramagnetic. Only in a small window, for a Fermi level between 1.24 eV and 1.79 eV the paramagnetic positive charge state should prevail. Recently, Lingner *et al.* identified the $V_{\text{C-C}_{\text{Si}}}$ -complex by spin resonance experiments in neutron-irradiated n-type 6H-SiC.²⁶ The hyperfine structure of an excited high spin state ($S = 1$) of this complex was detected using the magnetic dichroism of the adsorption (MCDA) and MCDA-EPR. The theoretical analysis showed that the excited state is related to an intra-defect excitation of $(V_{\text{C-C}_{\text{Si}}})^{2+}$, which is not paramagnetic in its ground state and therefore could not be detected by standard EPR. This is consistent with the observation of Itoh *et al.* The complex appeared only in samples annealed above the temperature at which the T1-center in 3C-SiC finally vanishes. EPR-centers with a similar g -tensor and fine structure constant D were observed earlier in n-type 6H-SiC⁵⁶ (P6- and P7-centers) and in electron irradiated nominally undoped 3C-SiC (L3-center).²⁷ The similarity suggests that the carbon vacancy-antisite complex as a common model for all these centers. Indeed, the annealing study of Son *et al.* shows that the center appears only after an annealing at 700°C-750°C. These observation support our interpretation of the annealing stages for the silicon vacancy reported by Itoh *et al.* An diffusion-based annealing mechanism, that was proposed earlier,^{17,27} is apparently not involved in these experiments.

Using PAS Kawasuso *et al.*^{10,12} have observed the annealing of vacancy-related defects in electron-irradiated n-type 3C-SiC and 6H-SiC. Two lifetime components were extracted from the positron signal in 6H-SiC. One component was attributed to defects related to silicon vacancies.^{18,19} The other was shown to originate from carbon vacancy-related defects. In 3C-SiC only the component corresponding to silicon vacancy-related defects was detected. Kawasuso *et al.* found that this lifetime component annealed in several stages. For annealing

temperatures below 500°C two annealing stages were observed in 3C- and 6H-SiC that followed the findings for the T1-center in 3C-SiC. In 3C-SiC vacancy-related defects were not detected above the annealing temperature of the T1-center. This finding is also consistent with our interpretation of the annealing stages, since a positive carbon vacancy-antisite complex would repel the positron and therefore should not contribute to the positron lifetime.

In 6H-SiC, however, the signal persisted the annealing at 750°C and finally annealed at 1450°C. Yet, an annealing stage with a less pronounced drop of the vacancy concentration is present at 750°C. In a more recent PAS-study⁶ using electron irradiated n-type 6H-SiC Kawasuso *et al.* describes the annealing of the silicon vacancy or related defect complexes with the a major stages at 500°C-700°C and 1000°C-1200°C. The vacancy-signature reached the bulk-level at 1200°C. In comparison to this more recent study, the samples of the earlier study had a larger nitrogen concentration (carrier density of $5.5 \times 10^{17} \text{ cm}^{-3}$ at room temperature vs. $5 \times 10^{15} \text{ cm}^{-3}$) and were irradiated with more energetic electrons at a lower dose ($1 \times 10^{17} e^-/\text{cm}^2$ at 3 MeV compared $3 \times 10^{17} e^-/\text{cm}^2$ at 2 MeV and). The differences in the annealing behavior is most likely related to these variation in the nitrogen concentrations and the irradiation conditions.

In the following we comment on presence of the annealing stages above 1000°C in 6H-SiC. In their analysis of the earlier experiment Kawasuso *et al.* explained the final annealing stage at 1450°C in terms of the dissociation of vacancy-nitrogen complexes and the subsequent annealing of the vacancy by out-diffusion or diffusion to sinks. The $V_{\text{Si}}\text{-N}$ complexes were expected to form during the annealing. Such an interpretation is plausible as similar positron lifetimes are predicted for the $V_{\text{Si}}\text{-N}$ complexes and the silicon vacancy.¹⁸ Very recent theoretical investigations show that these complexes are thermally stable in agreement with EPR-experiments.^{57,58} Yet, also the transformation into the carbon vacancy-antisite complex may play a relevant role in the PAS experiments, provided that the sample remains compensated (Fermi level around 1.7 eV) and that the positron annihilation at the carbon vacancy-antisite complex resembles that for the silicon vacancy. Precise calculations based on *ab initio* methods for this center are lacking sofar. However, calculations⁵⁹ using an approximate method based on the superposition of atomic densities (c.f. Ref. 60) using the atomic coordinates obtained for $V_{\text{C}}\text{-C}_{\text{Si}}$ obtained in our work indicate for 4H-SiC, that the positron lifetime associated with this center lie in the range similar to the value of the silicon vacancy (at the cubic site between 162 ps to 175 ps and at the hexagonal site 187 ps to 193 ps depending on the charge state). Thus the positron lifetime does not significantly change when the negative silicon vacancy transforms into the neutral hexagonal vacancy-antisite complex. The migration of the carbon vacancy-antisite complex is associated with larger barriers than

the transformation and hence is activated at higher temperatures. This scenario is a plausible explanation of the observed annealing of the V_{Si} -related signature in the PAS experiments, since the complex at the hexagonal site may become neutral during the annealing of compensating centers in n-type 4H-SiC. Obviously, Fermi level effects are relevant. The annealing characteristics should therefore depend on the polytype (due to the different band gap width). Based on our present understanding, we do not exclude the formation of vacancy-nitrogen complexes as an explanation of the final annealing stage. The interpretation of the last annealing stage in terms of vacancy-nitrogen complexes, however, requires that the dopant is present in similar or higher concentrations than the vacancies at the onset of the annealing stage.

B. Carbon vacancies and interstitials

For the carbon vacancy the annealing hierarchy starts with the vacancy-interstitial recombination at the first annealing stage and ends with the diffusion of vacancies to sinks or its out-diffusion (c.f. Fig. 1). The recombination of Frenkel pairs containing the carbon split-interstitial as the nearest or second neighbor of the vacancy proceeds with lower recombination barriers than the vacancy diffusion. Similarly the migration barrier for the carbon split-interstitial is lower than for the carbon vacancy. For the vacancy-interstitial recombination, the migration of the interstitial towards the vacancy is the bottle neck, since recombination of the nearest or second neighbor Frenkel pairs proceeds with a similar or lower barrier. The annealing of the vacancy based on its diffusion therefore should be activated at much higher temperatures than the vacancy-interstitial recombination.

In irradiated material, where interstitials and vacancies are present in similar concentrations, we expect the vacancy-interstitial recombination to represent the first annealing stage. Our finding of a relevant binding energy for all charge states of the nearest and second neighbor Frenkel pair suggests an attractive interaction that traps the interstitial in the vicinity of the vacancy. Hence, we expect that a recombination of these Frenkel pairs has a higher probability than their dissociation. However, the diffusion-limited recombination of the isolated defects may be hindered by a Coulomb repulsion of the charged defects. This occurs only in p-type material for a Fermi level below 0.8 eV (cf. Tab. I). Above this value the carbon split-interstitial is neutral. Even though the split-interstitial becomes negative in n-type 3C-SiC, the vacancy should remain neutral. For n-type 4H-SiC, on the other hand, our calculations show that also the carbon vacancy becomes negative as a consequence of the larger band gap. The additional Coulomb barrier in p-type 3C-SiC and p-type or n-type 4H-SiC may leave a considerable fraction of vacancies unannealed in this first annealing stage. At the same time the carbon split-interstitials could anneal by diffusion to other defects where ther-

mally stable defects complexes or defect clusters could be formed. The remaining vacancies anneal in a second annealing stage based on the vacancy diffusion.

So far the isolated carbon vacancy was not detected by EPR-experiments nor by PAS experiments in irradiated 3C-SiC. A spin resonance center T5 was observed together with the T1-center (V_{Si}^-) by Itoh *et al.* that annealed at 150°C. Its hyperfine (HF) signature originates from four silicon atoms and it was therefore identified as a defect on the carbon sublattice. However, the original assignment to the positive carbon vacancy had been revised to a complex of two hydrogen atoms with a carbon vacancy,^{61,62} given the D_2 -symmetry of the center that is incompatible with the theoretical findings^{48,49} for the carbon vacancy. Based on the calculations of HF-parameters for these models and the carbon split-interstitial it was recently shown that only the split-interstitial may explain the experimental findings for the T5-center.^{23,24,63,64} Such an identification of the T5-center has to be verified experimentally, as the carbon HF-tensors of the $\langle 100 \rangle$ -oriented carbon dumbbell have so far not been observed. Yet, this model would explain the low annealing temperature of the T5-center. According to our analysis the positive carbon split-interstitial is indeed a highly mobile defect, with a migration barrier of only 0.9 eV. A comparison of the ionization levels of this defect and V_{Si} (cf. Tab. I) shows that $C_{\text{sp}\langle 100 \rangle}^+$ and V_{Si}^- simultaneously exist in a paramagnetic state for a Fermi-level around 0.7 eV in the p-type samples which is in agreement with the simultaneous observation of the T1- and T5-center.¹⁷ At these doping conditions the carbon vacancy prevails in the non-paramagnetic doubly positive charge state. This explains why the carbon vacancy was not detected in EPR experiments or by PAS (the positron recombination at the positive vacancy is suppressed by the Coulomb repulsion). Therefore the mechanism (vacancy-interstitial recombination or other diffusion-limited mechanisms) behind the annealing of the T5-center cannot be deduced from the present experiments.

A competing process to the vacancy-interstitial recombination is the formation of carbon interstitial clusters as discussed in Sec. V. Due to their high dissociation energies such clusters would emit interstitials only at elevated annealing temperatures. These interstitials then take part in further defect reactions. For the di-interstitial and the tri-interstitial in 3C-SiC a dissociation energy of 3 eV plus an additional barrier, which may be approximated by the migration barrier of the interstitial (0.5 eV for $C_{\text{sp}\langle 100 \rangle}^0$), is needed to remove a carbon atom. This activation barrier is only slightly lower than the migration barrier of the carbon vacancy (4.1 eV for V_{C}^+ and 3.5 eV for V_{C}^0). With a dissociation barrier of 5.7 eV the tetra-interstitial is much more stable and should emit interstitials at higher temperatures than the di- and tri-interstitial. A comparison of the dissociation energies with the activation energies of the other processes suggests that new carbon interstitials should be supplied

at temperatures above 1000°C. Indeed, the concentration of e.g. the photo-luminescence centers D_{I}^2 and D_{II}^4 , which are presumably related to antisites^{65,66} and carbon aggregates,^{4,67} rises significantly at annealing temperatures above 1000°C.^{3,8} For both formation processes the availability of free carbon atoms is an important prerequisite.^{65,67} Defects similar to the carbon clusters described here are known from other semiconductors. Besides the carbon clusters in diamond⁵² one can also mention here the well known $\{311\}$ -interstitial defects in silicon. These defects emit silicon interstitials and thereby drive the transient enhanced diffusion of dopants during the annealing.⁶⁸

In contrast to 3C-SiC, the signatures of the carbon vacancy and interstitial were reported in 4H-SiC. In irradiated p-type 4H-SiC, recently two EPR-centers (EI1 with $S=1/2$ and EI3 with $S=1$) were identified by Son *et al.* (Ref. 69) that possess a similar g -tensor as the T5-center in 3C-SiC. The analysis of the HF-signature showed that the defects are located on the carbon sublattice. Theoretical calculations indicate that the observed silicon HF-tensors are consistent with the theoretical values for the positive and neutral carbon split-interstitial, respectively.^{47,63,64} Similar to the T5-center the EI1 and EI3 center anneal around 200°C. In p-type 4H-SiC irradiated at 400°C Son *et al.*^{16,69} observed by EPR-experiments the final disappearance of the EI5-center at 500°C. The center was tentatively assigned to a positive carbon vacancy. This assignment was verified by calculations of HF-tensors,^{22,23,47} and it was shown that the center is located at the cubic site. The low annealing temperature of the EI5-center is consistent with our discussion of the vacancy-interstitial recombination in 3C-SiC. The observation of only a single annealing stage for the carbon vacancy in the EPR-experiments is also consistent with PAS experiments¹⁰ performed in irradiated 6H-SiC. There it was found that the corresponding lifetime component annealed at 500°C.

Recently, Konovalov *et al.*,²⁰ Zvanut and Konovalov,⁷⁰ and Son *et al.*⁷¹ have studied EPR-centers in semi-insulating 4H-SiC. They identified the centers ID1 (Refs. 20,70) and EI5 (Ref. 71). The latter was already observed in irradiated 4H-SiC. The center ID1 resembles the EI5 center with respect to its g -tensor and HF-values, which suggest a common identification as a carbon vacancy at the cubic lattice site.²⁴ Both centers possess a higher thermal stability than the EI5-center in irradiated SiC. For example Konovalov *et al.* have found that the center persists up to 850°C.²⁰ The material used by Konovalov *et al.* and Zvanut and Konovalov was high purity, as-grown (0001) 4H-SiC wafers grown by the seeded sublimation method. The high temperatures (> 2000 °C) applied during growth suggest that intrinsic defects are present in the material close to their equilibrium abundance. This means that carbon vacancies by far outnumber carbon interstitials, due to the much lower formation energy of the vacancy as compared to the interstitial. Also, the concentration of carbon interstitial clusters is

predicted to be well below the vacancy concentration. Therefore the excess concentration of carbon vacancies in a material grown at high temperatures may reach its equilibrium concentration at lower temperature only by a mechanism based on the vacancy diffusion. The large migration barrier of the carbon vacancy – 4.1 eV for V_C^+ in 3C-SiC – explains the high thermal stability of carbon vacancies in as-grown semi-insulating samples.

VII. SUMMARY AND CONCLUSION

The microscopic picture of the annealing mechanisms of vacancies and interstitials has been developed from theoretical investigations based on ab initio methods within the framework of DFT. We analyzed in detail the ground state configurations of Frenkel pairs formed by carbon (silicon) vacancies and interstitials and calculated the recombination barriers. We investigated the capture (and emission) of carbon interstitials by (from) carbon interstitial clusters. Various clusters involving up to four carbon interstitials were considered and the energy needed to emit single carbon interstitials from these clusters was calculated.

A hierarchy of annealing mechanisms has been derived that places the vacancy-interstitial recombination and the carbon clustering into context with diffusion based mechanisms and the metastability of the silicon vacancy. The recombination barriers and dissociation energies were compared with the barriers of interstitial and vacancy migration as well as the transformation barrier of the silicon vacancy. The relevance of the Fermi-level effect was demonstrated for the annealing hierarchy of the silicon vacancy and interstitial. The effect originates from two distinct configurations of the silicon interstitial in p-type and compensated (or n-type) material and the stabilization of the silicon vacancy in n-type material. In both cases a strong variation of the migration and transformation barriers with the Fermi-level is observed, which changes the hierarchical ordering of the annealing mechanisms. While in compensated material the vacancy-interstitial recombination and the diffusion-based annealing of silicon interstitials are activated at lower temperatures than the metastability-related annealing of the silicon vacancy, this ordering is reversed in p-type mate-

rial. In n-type material the metastability-based annealing is unavailable and a diffusion-based mechanism is observed instead. Regarding the annealing of carbon interstitials and vacancies, the highly mobile carbon interstitials were shown to drive the vacancy-interstitial recombination and the formation of thermally stable carbon-interstitial clusters at the early stage of the annealing. The comparably low mobility of the carbon vacancy permits its diffusion-based annealing only at elevated temperatures. In this case, the hierarchical ordering was found to be independent of the Fermi-level effect. The emission of carbon interstitials from carbon interstitial-clusters is associated with activation energies that exceed the activation energies of the vacancy migration. Thus the clusters can provide carbon interstitials even at temperatures at which isolated carbon vacancies have vanished.

The annealing hierarchy was discussed in the light of annealing experiments on EPR- and PAS-centers, supported by the recent microscopic identification of these centers through experimental and theoretical analysis. A consistent interpretation of the present experimental data for 3C-SiC is facilitated by the proposed annealing hierarchy. The available experiments and theoretical work for 4H- and 6H-SiC suggest that our qualitative conclusions should (with limitations) apply to other polytypes. We hope to stimulate further experimental investigation of the defects' annealing kinetics with our analysis. In particular, the annealing stages of the silicon vacancy above 1000°C and the confirmation of the tentative assignment of the EPR-centers T5, EI1 and EI2 to carbon interstitials call for further clarification. Also the role of defect aggregates, as exemplified by carbon interstitials, needs experimental substantiation. These aggregates should provide the missing link between the kinetics of the primary defects and the thermally stable PL-centers.

Acknowledgments

Fruitful discussions with G. Pensl, W.J. Choyke, M.E. Zvanut and N.T. Son are gratefully acknowledged. This work has been supported by the Deutsche Forschungsgemeinschaft within the SiC Research Group.

¹ W. J. Choyke and L. Patrick, Phys. Rev. B **4**, 1843 (1971).
² L. Patrick and W. J. Choyke, Phys. Rev. B **5**, 3253 (1972).
³ T. Egilsson, J. P. Bergman, I. G. Ivanov, A. Henry, and E. Janzén, Phys. Rev. B **59**, 1956 (1999).
⁴ L. Patrick and W. J. Choyke, J. Chem. Phys. Solids **34**, 565 (1973).
⁵ S. G. Sridhara, D. G. Nizhner, R. P. Devaty, W. J. Choyke, T. Dalibor, G. Pensl, and T. Kimoto, Mater. Sci. Forum **264-268**, 495 (1998).
⁶ A. Kawasuso, F. Redmann, R. Krause-Rehberg, T. Frank,

M. Weidner, G. Pensl, P. Sperr, and H. Itoh, J. Appl. Phys. **90**, 3377 (2001).
⁷ G. A. Evans, J. W. Steeds, L. Ley, M. Hundhausen, N. Schulze, and G. Pensl, Phys. Rev. B **66**, 35204 (2002).
⁸ J. A. Freitas, G. Bishop, J. A. Edmond, J. Ryu, and R. F. Davis, J. Appl. Phys. **61**, 2011 (1987).
⁹ T. Egilsson, A. Henry, I. G. Ivanov, J. L. Lindström, and E. Janzén, Phys. Rev. B **59**, 8008 (1999).
¹⁰ A. Kawasuso, H. Itoh, S. Okada, and H. Okumura, J. Appl. Phys. **80**, 5639 (1996).

- ¹¹ G. Brauer, W. Anwand, P. G. Coleman, A. P. Knights, F. Plazaola, Y. Pacaud, W. Skorupa, J. Störmer, and P. Willutzki, *Phys. Rev. B* **54**, 3084 (1996).
- ¹² A. Kawasuso, H. Itoh, N. Morishita, M. Yoshikawa, and T. Ohshima, *Appl. Phys. A* **67**, 209 (1998).
- ¹³ A. Polity, S. Huth, and M. Lausmann, *Phys. Rev. B* **59**, 10603 (1999).
- ¹⁴ T. Wimbauer, B. K. Meyer, A. Hofstaetter, A. Scharmann, and H. Overhof, *Phys. Rev. B* **56**, 7384 (1997).
- ¹⁵ H. J. von Bardeleben, J. L. Cantin, L. Henry, and M. F. Barthe, *Phys. Rev. B* **62**, 10841 (2000).
- ¹⁶ N. T. Son, P. N. Hai, and E. Janzén, *Phys. Rev. B* **63**, 201201 (2001).
- ¹⁷ H. Itoh, A. Kawasuso, T. Ohshima, M. Yoshikawa, I. Nashiyama, S. Tanigawa, S. Misawa, H. Okumura, and S. Yoshida, *phys. stat. sol. (a)* **162**, 173 (1997).
- ¹⁸ G. Brauer, W. Anwand, E.-M. Nicht, J. Kuriplach, M. Sob, N. Wagner, P. G. Coleman, M. J. Puska, and T. Korhonen, *Phys. Rev. B* **54**, 2512 (1996).
- ¹⁹ T. E. M. Staab, L. M. Torpo, M. J. Puska, and R. M. Nieminen, *Mater. Sci. Forum* **353-356**, 533 (2001).
- ²⁰ V. V. Konovalov, M. E. Zvanut, V. F. Tsvetkov, J. R. Jenny, S. G. Müller, and H. M. Hobsgood, *Physica B* **308-310**, 671 (2001).
- ²¹ V. Y. Bratus, I. N. Makeeva, S. M. Okulov, T. L. Petrenko, T. T. Petrenko, and H. von Bardeleben, *Physica B* **309-310**, 621 (2001).
- ²² T. T. Petrenko, T. L. Petrenko, V. Y. Bratus, and J. L. Monge, *Physica B* **308-310**, 637 (2001).
- ²³ M. Bockstedte, M. Heid, A. Mattausch, and O. Pankratov, *Mater. Sci. Forum* **389-393**, 471 (2002).
- ²⁴ M. Bockstedte, M. Heid, and O. Pankratov, *Phys. Rev. B* **67**, 193102 (2003).
- ²⁵ A. Kawasuso, H. Itoh, T. Ohshima, K. Abe, and S. Okada, *J. Appl. Phys.* **82**, 3232 (1997).
- ²⁶ T. Lingner, S. Greulich-Weber, J.-M. Spaeth, U. Gerstmann, E. Rauls, Z. Hajnal, T. Frauenheim, and H. Overhof, *Phys. Rev. B* **64**, 245212 (2001).
- ²⁷ N. T. Son, E. Sörman, W. M. Chen, C. Hallin, O. Kordina, B. Monemar, E. Janzén, and J. L. Lindström, *Phys. Rev. B* **55**, 2863 (1997).
- ²⁸ E. Rauls, T. Lingner, Z. Hajnal, S. Greulich-Weber, T. Frauenheim, and J.-M. Spaeth, *phys. stat. sol. (b)* **217**, R1 (2000).
- ²⁹ M. Bockstedte and O. Pankratov, *Mater. Sci. Forum* **338-342**, 949 (2000).
- ³⁰ N. Son, B. Magnusson, Z. Zolnai, A. Ellison, and E. Janzén, *Mater. Sci. Forum* **433-436**, 45 (2003).
- ³¹ M. Bockstedte, A. Kley, J. Neugebauer, and M. Scheffler, *Comp. Phys. Comm.* **200**, 107 (1997).
- ³² P. Hohenberg and W. Kohn, *Phys. Rev.* **136B**, 864 (1964).
- ³³ W. Kohn and J. L. Sham, *Phys. Rev.* **140A**, 1133 (1965).
- ³⁴ J. P. Perdew and A. Zunger, *Phys. Rev. B* **23**, 5048 (1981).
- ³⁵ D. M. Ceperley and B. J. Alder, *Phys. Rev. Lett.* **45**, 566 (1980).
- ³⁶ H. J. Monkhorst and J. D. Pack, *Phys. Rev. B* **13**, 5188 (1976).
- ³⁷ G. Makov and M. C. Payne, *Phys. Rev. B* **51**, 4014 (1995).
- ³⁸ J. Lento, J.-L. Mozos, and R. M. Nieminen, *J. Phys. Cond. Matt.* **14**, 2637 (2002).
- ³⁹ M. Bockstedte, A. Mattausch, and O. Pankratov, *Phys. Rev. B* in print.
- ⁴⁰ N. Troullier and J. L. Martins, *Phys. Rev. B* **43**, 1993 (1991).
- ⁴¹ M. Fuchs and M. Scheffler, *Comp. Phys. Comm.* **119**, 67 (1999).
- ⁴² A carbon pseudopotential with the following matching radii is used: $r_s^c=1.6$ Bohr, $r_p^c=1.7$ Bohr and $r_d^c=1.5$ Bohr.
- ⁴³ G. A. Baraff, E.O. Kane, and M. Schlüter, *Phys. Rev. Lett.* **43**, 956 (1979).
- ⁴⁴ E. Pehlke and P. Kratzer (2000), priv. commun.
- ⁴⁵ I. V. Ionova and E. A. Carter, *J. Chem. Phys.* **98**, 6377 (1993).
- ⁴⁶ A. Mattausch, M. Bockstedte, and O. Pankratov, *Mater. Sci. Forum* **353-356**, 323 (2001).
- ⁴⁷ M. Bockstedte, M. Heid, A. Mattausch, and O. Pankratov, *Mater. Sci. Forum* **433-436**, 471 (2003).
- ⁴⁸ A. Zywiets, J. Furthmüller, and F. Bechstedt, *Phys. Rev. B* **59**, 15166 (1999).
- ⁴⁹ L. Torpo, M. Marlo, T. E. M. Staab, and R. M. Nieminen, *J. Phys. Cond. Matt.* **13**, 6203 (2001).
- ⁵⁰ E. Rauls, T. E. M. Staab, Z. Hajnal, and T. Frauenheim, *Physica B* **308-310**, 645 (2001).
- ⁵¹ L. Torpo, T. E. M. Staab, and R. M. Nieminen, *Phys. Rev. B* **65**, 85202 (2002).
- ⁵² J. P. Goss, B. J. Coomer, R. Jones, T. D. Shaw, P. R. Briddon, M. Rayson, and S. Öberg, *Phys. Rev. B* **63**, 195208 (2001).
- ⁵³ A. Mattausch, M. Bockstedte, and O. Pankratov, unpublished.
- ⁵⁴ J. Bourgoin and M. Lannoo, *Point Defects in Semiconductors II*, vol. 35 of *Springer Series in Solid-State Sciences* (Springer Verlag, Berlin, 1983).
- ⁵⁵ H. Itoh, N. Hayakawa, I. Nashiyama, and E. Sakuma, *J. Appl. Phys.* **66**, 4529 (1989).
- ⁵⁶ V. S. Vainer and V. A. Il'in, *Sov. Phys. Solid. State* **23**, 2126 (1981).
- ⁵⁷ U. Gerstmann, E. Rauls, T. Frauenheim, and H. Overhof, *Phys. Rev. B* **67**, 205202 (2003).
- ⁵⁸ V. S. Vainer and V. A. Il'in, *Sov. Phys. Solid State* **23**, 1432 (1981).
- ⁵⁹ A. Kawasuso, priv. commun.
- ⁶⁰ M. J. Puska and R. M. Nieminen, *Rev. Mod. Phys.* **66**, 841 (1994).
- ⁶¹ B. Aradi, A. Gali, P. Deák, J. E. Lowther, N. T. Son, E. Janzén, and W. J. Choyke, *Phys. Rev. B* **63**, 245202 (2001).
- ⁶² A. Gali, B. Aradi, P. Deák, W. J. Choyke, and N. T. Son, *Phys. Rev. Lett.* **84**, 4926 (2000).
- ⁶³ T. T. Petrenko, T. L. Petrenko, and V. Y. Bratus, *J. Phys. Cond. Matt.* **14**, 12433 (2002).
- ⁶⁴ A. Gali, P. Deák, N. T. Son, E. Janzén, H. J. von Bardeleben, and J.-L. Monge, *Mater. Sci. Forum* **433-436**, 511 (2003).
- ⁶⁵ T. A. G. Eberlein, C. J. Fall, R. Jones, P. R. Briddon, and S. Öberg, *Phys. Rev. B* **65**, 184108 (2002).
- ⁶⁶ A. Gali, P. Deák, E. Rauls, N. T. Son, I. G. Ivanov, F. H. C. Carlsson, E. Janzén, and W. J. Choyke, *Phys. Rev. B* **67**, 155203 (2003).
- ⁶⁷ A. Mattausch, M. Bockstedte, and O. Pankratov, *Physica B* **308-310**, 656 (2001).
- ⁶⁸ D. J. Eaglesham, P. A. Stolk, H.-J. Gossmann, and J. M. Poate, *Appl. Phys. Lett.* **65**, 2305 (1994).
- ⁶⁹ N. T. Son, P. N. Hai, and E. Janzén, *Mater. Sci. Forum* **353-356**, 499 (2001).
- ⁷⁰ M. E. Zvanut and V. V. Konovalov, *Appl. Phys. Lett.* **80**, 410 (2002).
- ⁷¹ N. T. Son, B. Magnusson, and E. Janzén, *Appl. Phys. Lett.*

81, 3945 (2002).